TWENTYFIFTH EUROPEAN ROTORCRAFT FORUM

Paper n° B11

NUMERICAL SIMULATION of 2D BLADE VORTEX INTERACTION USING MOVING OVERSET GRIDS

BY

C.BENOIT

SEPTEMBER 14-16, 1999
R O M E
ITALY

ASSOCIAZIONE INDUSTRIE PER L'AEROSPAZIO, I SISTEMI E LA DIFESA
ASSOCIAZONE ITALIANA DI AERONAUTICA ED ASTRONAUTICA

NUMERICAL SIMULATION OF 2D BLADE VORTEX INTERACTION USING MOVING OVERSET GRIDS

C. Benoit
ONERA, CFD and Aeroacoustics Department
BP 72, 92322 Châtillon, France

Abstract. This paper presents the unsteady inviscid flow simulation of 2D blade-vortex interaction using a new mesh adaptation method. This method consists in overlapping automatically analytical moving grids to a given background grid (or set of grids). Refined grids are taken from a set of general grids, constructed from Bezier curves. The refined grid generation is based on the resolution of global optimization problems. Transfer of information between grids is Chimera-like in nature and is augmented with a correction. The method is first validated for steady airfoil and pure vortex advection calculations, before being applied to a blade-vortex interaction problem.

1 Introduction

Blade-vortex interaction is an important feature of helicopter aerodynamics since one blade of the rotor generally crosses the wake and tip vortex generated by the previous blade. Such a phenomena is highly undesirable from the aerodynamic and acoustic point of view. First, the vortex modifies the incoming flow and creates a sudden change in blade loading. Secondly, the impact of the vortex on the blade generates a noisy acoustic wave. Both of these two effects must be controlled by the helicopter designer to gain manoeuvrability and reduce noise.

The prediction of blade-vortex interaction (BVI) for rotorcraft is of particular interest for the helicopter industry. Of course, numerous experimental, theoretical and numerical studies are devoted to correctly predict the BVI. In recent years, advances in computer hardware have made the investigation of this problem possible using CFD methods.

However, CFD methods are far from being able to predict this kind of interaction for realistic rotorcraft applications. As a matter of fact, the rotorcraft flowfield is very complicated: unsteady, highly threedimensional and transonic at the blade tip. Besides, CFD methods lack of efficiency for this problem: classical numerical schemes are too dissipative and a static mesh that would be satisfactory during the complete computation without requiring an excessive number of grid points is difficult (if not impossible) to generate.

In this paper, we propose a new mesh strategy as an alternative to classical CFD tools and apply it to a model problem of BVI.

We chose to study a 2D blade-vortex interaction using the Euler equations. The helicopter blade is modeled by a NACA0012 profile and a vortex model is used to simulate the impacting vortex generated by the previous blade at initial time. This twodimensionnal test problem can be viewed as a limiting case when the vortex path is parallel to the blade.

To overcome the difficulties linked to classical vortex capturing CFD methods, there are several alternatives. Highly accurate schemes [14] allow one to diminish the numerical dissipation but they increase the required CPU time per cell and require extended boundary conditions.

Another approach is to use a local Eulerian/Lagrangian coupling method [9]. Using the Lagrangian equations to correct the Euler solution enables one to diminish numerical dissipation for advection problems but stability and conservation problems may arise.

A last alternative is to use automatic mesh adaptation. The advantage of this approach is that it can solve at the same time both the accuracy and the mesh construction problems.

In this paper, the 2D transonic, parallel BVI is investigated by solving the unsteady compressible Euler equations using a new mesh strategy based on overset moving grids, extensively described in [2]. The original feature of this method is that general structured overset fine grids are automaticaly generated by solving an optimization problem to adapt to the scale, shape and advection speed of the phenomena they are representing. In this approach, the numerical errors are decreased in three ways: by diminishing the size of mesh cell, by aligning the mesh lines with anisotropic phenomena such as shock waves and by moving the overset fine grids with an adapted speed and solving the equations in the grid-attached frames. This method enables us to obtain an accurate solution without increasing the computing time too much.

The proposed mesh method is derived from the Chimera technique [1] to take bodies and body motion into account and from the Adaptive Mesh Refinement (AMR) technique [3] for solution adaptation. Fine grids are automatically generated by solving a global optimization problem, that characterizes the equidistribution of the solution's error over the adapted mesh. This optimization problem is solved by a genetic algorithm [4],[8], modified with heuristics to increase its efficiency.

So the method can be viewed as an extension of the approach developed in [11], where moving overset grids were used but without automatic grid adaptation.

The first section of this paper will be dedicated to the description of the discretization scheme, The second part will be concerned with steady mesh adaptation with application to the simulation of transonic flow around a NACA0012 airfoil. The last part will be dedicated to unsteady mesh adaptation, with application to the pure advection of a Lamb vortex and to the simulation of the 2D parallel blade-vortex interaction.

2 Discretization Scheme

2.1 Governing Equations

In the mesh strategy we use, fine grids are able to move relative to a background grid without deformation. So a formulation of the Euler equations for a moving domain Ω of boundary Γ is necessary. The Euler equations are formulated in integral law-form. All vectors are projected in a relative frame attached to a fine grid and the scalar components of the absolute velocity are used:

$$\frac{d}{dt}\int_\Omega w\,dx\,dy + \int_\Gamma (f\,dy - g\,dx) = \int_\Omega S\,dx\,dy \qquad (1)$$

where

$$\begin{gathered} w = [\rho, \rho u, \rho v, \rho E]^T \\ f = [\rho(u - s_x), \rho u(u - s_x) + p, \\ \rho v(u - s_x), \rho E(u - s_x) + pu]^T \\ g = [\rho(v - s_y), \rho u(v - s_y), \\ \rho v(v - s_y) + p, \rho E(v - s_y) + pv]^T \\ S = [0, \rho W v, -\rho W u, 0]^T \end{gathered}$$

The quantities ρ, $\vec{v} = (u, v)$, E are the density, absolute velocity and total specific energy of the fluid. The quantity $\vec{s} = (s_x, s_y)$ is the velocity of the fine grid and W is the norm of the rotation vector of the relative frame with respect to the absolute frame. The relationship between E and p is given by the equation of state for a polytropic gas,

$$p = (\gamma - 1)[\rho E - \frac{1}{2}\rho(u^2 + v^2)] \qquad (2)$$

2.2 Discretization of Equations

The Euler equations are discretized on classical structured curvilinear grids, using a finite volume approach and a Jameson like centered scheme [5], [7] of second order accuracy. The equations are advanced in time using a four-stage Runge Kutta explicit scheme. The simplified implicit stage due to Lerat *et al.* [6] increases the stability domain.

During the mesh adaptation process that will be described in detail later, some automatically generated fine grids may overlap a body. In order to take the influence of the body on those grids, a technique taken from the Chimera approach [1] is used. The points that lie inside the body are not updated and they are uncoupled from the others in the implicit stage.

3 Steady Mesh Adaptation

In this section, the method is decribed and applied to the simulation of the steady transonic flow around the NACA0012 airfoil at $M_\infty = 0.8$ and 0 degree of incidence.

3.1 Initial Mesh Generation

For this application, the method starts from two grids. One is a classical structured grid with "C" topology (called the background grid) and is made of 125×26 points. The other one is a fine bodyfitted grid, used to describe the profile precisely (see Fig. 1) and is made of 774×11 points. Both grids are generated by an hyperbolic grid generator [12].

The flow field is initialized with a constant value, corresponding to the freestream conditions.

At the external boundaries of the background grid, relationships based on characteristic theory are imposed. On the body, a slip condition is set. For the external boundaries of the bodyfitted grid, relationships are given by interpolation of the flowfield from the background grid, and are hence not globally conservative.

3.2 Mesh Adaptation

The background grid is too coarse to provide an accurate solution and needs to be adapted based on the numerical solu-

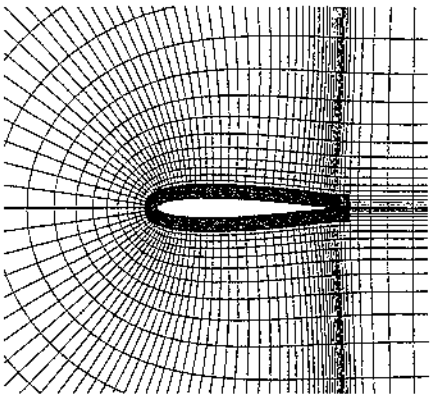

Figure 1: Initial mesh

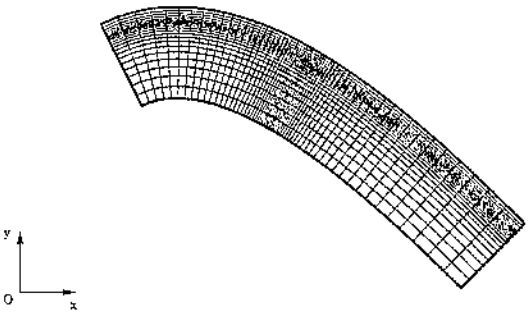

Figure 3: Example of analytical grid.

Figure 2: Adaptation/integration cycles

tion. In the steady approach, the integration/remeshing cycles described in the Fig. 2 are used. The solution is evolved on each grid with a local time step. Periodically, a refinement indicator is computed. This indicator is based on a Richardson extrapolation and provides an estimate of the truncation and interpolation errors of the solution. Then, the automatic generation of fine grids occurs.

Adaptation consists essentially in two stages. The first one is the clustering stage. This operation enables one to create zones where the refinement indicator exceeds some specified real value, refered to here as the "resolution". The second stage of the adaptation process is the optimization stage. Fine grids are built in order to optimally equidistribute the indicator on the new adapted grid to the resolution value, on each previously found cluster of points.

The clustering stage is realized by an agglomerative algorithm. Points of the old mesh are clustered if they are neighbouring points, if they exceed the resolution and if the resulting cluster of point does not have an excessively complicated shape.

The optimization stage requires the resolution of a global optimization problem. This stage is nevertheless simplified by the fact that we use analytical grids as fine grids. Such grids are characterized by a finite number of parameters. For example, the grid shown in Fig. 3 is described by the coordinates of the control points of the Bezier curve it is built from, by the height of the grid and by some parameters controlling the distribution of points inside the grid (a total of 11 parameters). The idea is to find the best set of parameters for each grid on each cluster in order to equidistribute the indicator to the resolution value.

To measure the refinement indicator on the new mesh, an *a priori* estimator is used. The estimated indicator is proportional to the indicator on the old mesh and the proportionality ratio is equal to the cell volume of the new mesh divided by the cell volume of the old mesh.

We are left with solving explicitly the optimization problem. To do this, first, a good initial mesh is found by heuristic considerations (for ex: the grid should cover the zone where the indicator exceeds the resolution value). For some cases, these heuristics can be sufficient. To go further, an optimizer based on real coded genetic algorithms has also been used.

Once the fine grids are generated, the connectivity for information transfers is computed. If a grid crosses a body, some points of it are blanked. Points around blanked points are interpolated from another grid. The external boundaries of the fine grids are given by interpolation. The flowfield solution in the region of the background grid that is covered by fine grids is corrected by interpolation from the solution in these grids.

General interest of this approach. The major advantage of this technique is that only regular, anisotropicly

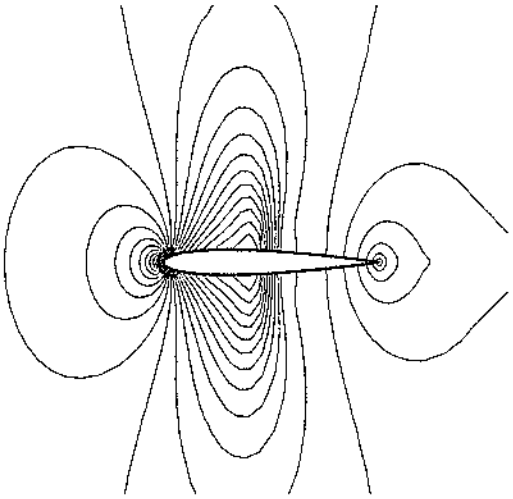

Figure 4: Iso-Mach lines for the steady computation on the background grid without adaptation

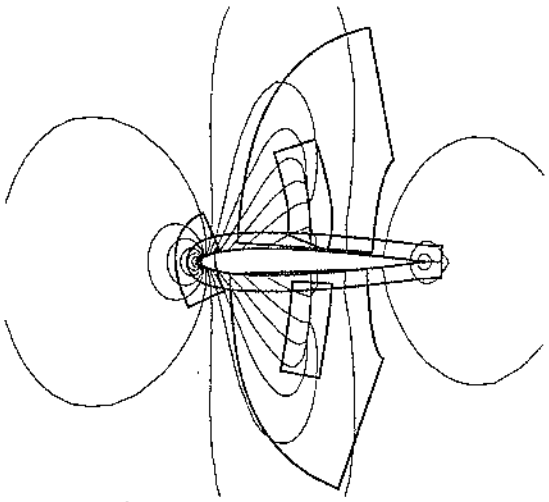

Figure 5: Iso-Mach lines for the steady computation on the adapted mesh

refined meshes with non negative volume are generated, since these properties are ensured through optimization constraints. The major drawback is that an extra stage is added (the optimization stage) compared to other mesh adaptation techniques such as AMR.

NACA0012 steady computation. The figure 4 shows the iso-Mach lines for the Euler solution obtained without adaptation on the background grid only. The figure 5 shows the iso-Mach lines obtained with the mesh adaptation method. This mesh is made of two levels of fine grids. It contains a grid at the leading edge and two grids covering shock waves. The complete mesh is made up of 51529 points. Bold contours show the boundaries of the grids composing this mesh.

Grids have been automatically generated to capture both shock waves and adjust themselves to fit their shape (Fig. 6). As a result, these features of the solution are well solved. In the figure 7, one can check that the solution is symmetrical, even if the mesh is not completely symmetrical.

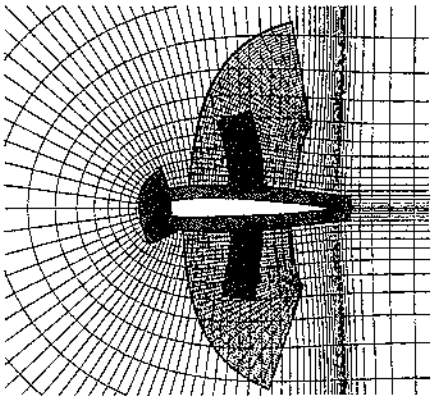

Figure 6: Adapted mesh

4 Unsteady Mesh Adaptation. Application to the Blade-Vortex Interaction.

In this section, we first present the additional features of the method for unsteady flow simulations. Then, we present ap-

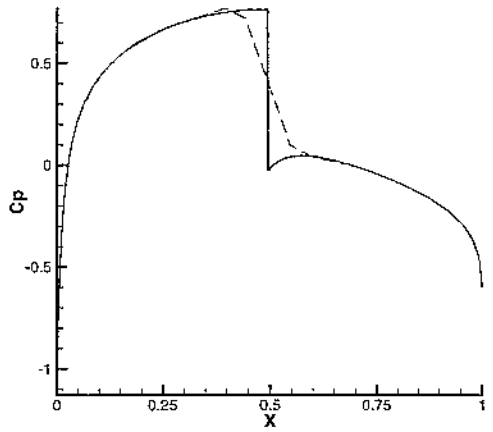

Figure 7: Pressure coefficient on the profile for the background grid (_ _ _) and for the adapted mesh (____)

plications to the advection of a Lamb vortex and to the blade-vortex interaction.

4.1 Mesh Adaptation

Unsteady mesh adaptation requires the same type of initial mesh as steady mesh adaptation, that is: a background set of grids and a bodyfitted set of grids. Besides, the same kind of cycles are used as before. The major differences are that we use a time accurate scheme to integrate the solution in time on each fine grid. The second one is that there is an additional stage to the algorithm called "speed optimization".

A speed is given to the adapted fine grids, such that they follow the phenomena they capture. This speed is determined by solving another optimization problem and is then used in the formulation of equations. The idea is to find the speed for the grid such that it covers the same shape in the composite refinement indicator field at two consecutive times.

General interest of this approach. This technique enables us to diminish much of the numerical dissipation for advection problems. Additionally, re-meshing can occur less often.

4.2 Vortex Advection

The simple test case of the pure advection of a Lamb vortex in an infinite domain at $M_\infty = 0.7$ is now presented. The vortex should be advected without deformation and dissipation. The background grid is made of 201×101 points.

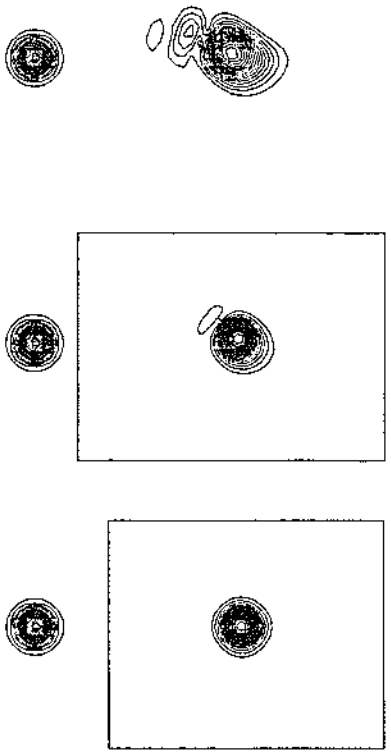

Figure 8: Vorticity without, with adaptation (but no speed optimization) and with complete adaptation

The figure 8 compares the solutions obtained on the background grid only (without adaptation), with adaptation but no speed optimization and with complete adaptation. We observe that automatically generated fine grids cover the vortex and the automatically detected speed is coherent with the normalized advection speed of the vortex, which is 0.7 (Fig. 9).

If we note p_c the pressure in the center of the vortex, we can define the numerical dissipation coefficient of the vortex at time t by:

$$1 - \frac{(p_\infty - p_c)_{(t)}}{(p_\infty - p_c)_{(t=0)}} \qquad (3)$$

In the following, we compute this coefficient for $t = 13, 1\mathcal{T}$ where $\mathcal{T}$ is the time taken by the vortex to travel one core radius.

Without adaptation the vortex is very deformed and dissipated. The numerical dissipation coefficient is equal to 60%. With refinement, the vortex is kept concentrated but is still deformed. The dissipation coefficient is equal to 26%.

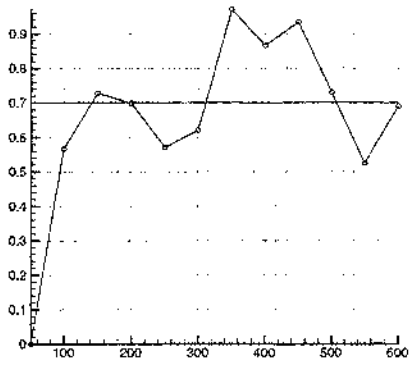

Figure 9: Automatically detected speed versus integration iterations.

With complete adaptation, the vortex is no longer deformed and dissipated very little (9%). Information on the pressure curves in a slice in the vortex core is given in Fig. 10.

Results are compared with those obtained with a completely refined cartesian grid with uniform cell size, corresponding to the smaller cell size of the adapted mesh and are summed up in the table 1. The computation in the refined cartesian grid is taken as a reference for the comparison of CPU times.

Mesh	Speed detec.	Number of points	CPU time	Dissipation coefficient
Backgrd grd	–	20301	0.03	60%
Fine grid	–	171875	1	7%
Adapted	no	26725	0.49	26%
Adapted	yes	22801	0.28	9%

Table 1: Sum up of results for Lamb vortex advection

4.3 Blade-Vortex Interaction

Next we present the simulation of the blade-vortex interaction. The test case we have computed here is borrowed from Srinivasan *et al* [13] and Ng and Hillier [10]. The blade section is represented by a NACA0012 profile and the vortex at initial time is modeled by the Scully relations. The freestream Mach number is set to $M_\infty = 0.8$.

To perform this computation, the flow field obtained previously around the NACA0012 is used. The initial field for BVI is obtained by superposition of this field and of a vortex field obtained by Scully's relationships. This process is detailed now.

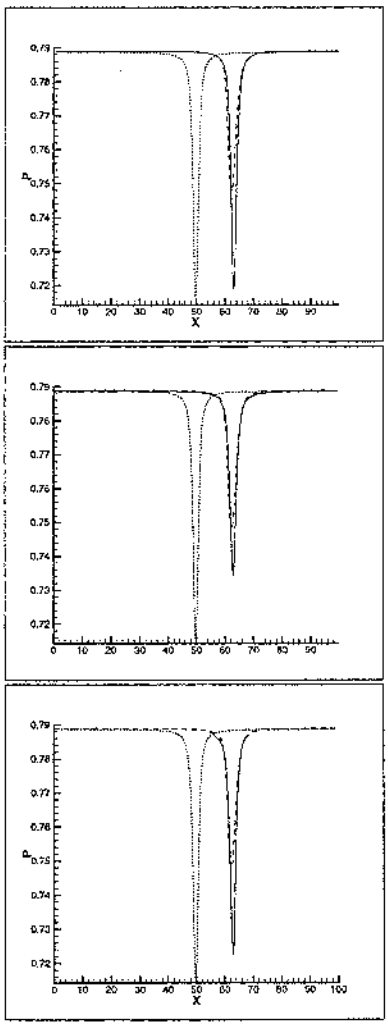

Figure 10: Pressure in a slice in the vortex core at $t = 13,1\mathcal{T}$ (——), at initial time (. . . .) and solution obtained on the background grid (_ _ _). From left to right: solution for a completely refined uniform cartesian grid, adapted mesh without speed optimization and complete adaptation.

4.3.a Initialization from the previous steady field

Scully's vortex

We first consider a Scully vortex in an infinite domain at $M_\infty = 0.8$. The initial velocity field is composed of a constant contribution and of another term coming from the vortex.

$$\mathbf{u} = \mathbf{u}_\infty + v_\theta \mathbf{e}_\theta \tag{4}$$

where $\mathbf{e}_\theta$ is the tangential vector of the cylindrical frame.

The tangential velocity of the vortex is given by:

$$v_\theta(r) = \frac{\Gamma}{2\pi} \frac{r}{r^2 + a^2} \tag{5}$$

where a is the radius of the vortex core, r is the distance to the center of the vortex and Γ is the vortex circulation.

The pressure is given by integration of the radial momentum equation (written in the vortex frame):

$$\frac{dp}{dr} = \frac{\rho v_\theta^2}{r} \tag{6}$$

If we suppose that the temperature is constant in the vortex core:

$$\text{for } r \leq a, p = \rho r T \tag{7}$$

and that out of the core:

$$\text{for } r \geq a, p = \text{cste}\, \rho^\gamma \tag{8}$$

In the forthcoming numerical simulation of blade-vortex interaction, the values for the normalized vortex circulation will be set to $0.2\, u_\infty$ and the normalized vortex core radius will be set to 0.05.

Field superposition

Note that $\rho_N, p_N ...$ refer to the steady flow quantities obtained previously around the NACA0012 airfoil. Note that $\rho_V, p_V ...$ refer to the flow quantities for the isolated Scully's vortex.

To obtain the initial field for the BVI simulation, the velocity of these two flow fields are summed (this is not a problem since the flowfield around the NACA0012 airfoil is constant in the region where the vortex is introduced):

$$\mathbf{u} = \mathbf{u}_V + \mathbf{u}_N \tag{9}$$

Then, the density fields are superposed in order to find the conditions at infinity for the interactional problem (corresponding to $M_\infty = 0.8$):

$$\rho = \rho_V + \rho_N - \rho_\infty \tag{10}$$

The same thing is done for the pressure:

$$p = p_V + p_N - p_\infty \tag{11}$$

Since we need to have a precise initial solution, a fine cartesian grid is added to the adapted mesh obtained previously, which locally covers the vortex.

4.3.b Results and discussion for BVI

Results have been obtained for an offset Δ between the vortex and the airfoil equal to $0.26c$ (c denotes the chord of the profile) and the vortex is introduced at 4.5 chords from the leading edge of the profile. In this section, $\mathcal{T}$ is the time taken by the vortex to travel one chord of the profile.

After the introduction of the vortex, the main problems of this simulation are, on one hand, the control of the numerical dissipation of the vortex during its advection, and, on the other hand, the generation of an efficient mesh to reduce the required CPU time.

The method succeeded in creating an efficient mesh for this problem (see Fig. 11). Grid stretchings occur in the shock waves and vortex core. An accurate speed for the grid that covers the vortex has also been automatically determined. The method is shown to be able to raise the overall solution accuracy. These grids enable the accurate capturing of shock waves (Fig. 12 and 13) and of the interaction between the vortex and the shock. However, some spurious oscillations in the field appear during the crossing of the vortex.

The concentration of the vortex is kept high through all the computation (Fig. 14) thanks to the moving grids. This figure shows the deformation of the vortex core during the crossing of the shock.

The figure 15 and 16 show the influence of the vortex on the pressure coefficient on the profile. When the vortex is far from the profile, its influence results in the displacement of the shock wave at the upper surface toward the leading edge. When the vortex arrives at the leading edge, the pressure is decreased at the leading part of the profile. Finally, when the vortex crosses the shock, its influence is directely visible on the pressure coefficient curve.

5 Conclusion and Future work

We have presented an automatic mesh method that generates quite general adapted and moving overset grids and we have shown the interest of such an approach for the simulation of blade vortex interaction.

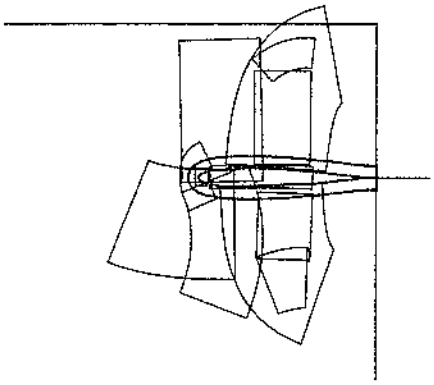

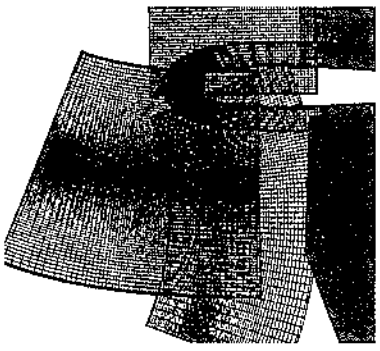

Figure 11: Grids boundaries at $t = 4,264\,\mathcal{T}$ and zoom on the automatically generated mesh at the leading edge

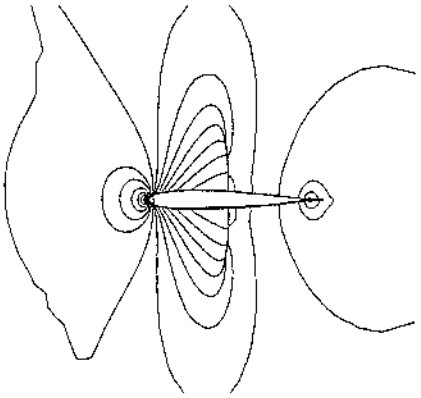

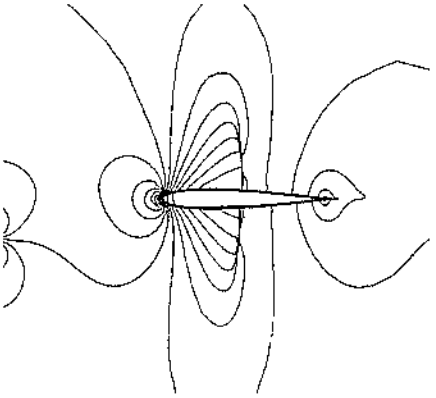

Figure 12: Iso-Mach lines at $t = 0,18\,\mathcal{T}$, $t = 3,264\,\mathcal{T}$ ($\Delta M = 0,055$).

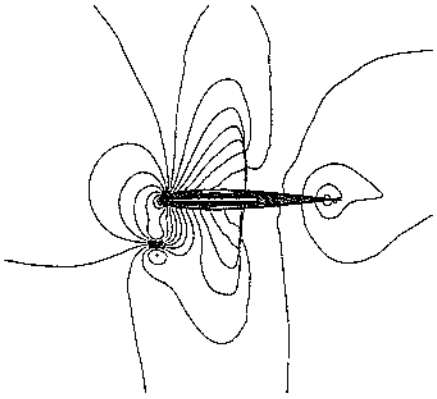

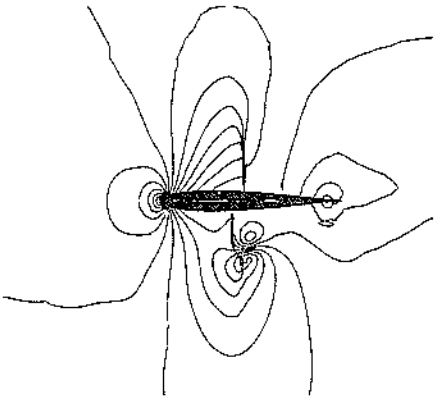

Figure 13: Iso-Mach lines at $t = 3,264\,\mathcal{T}$, $t = 4,264\,\mathcal{T}$ et $t = 5,02\,\mathcal{T}$ ($\Delta M = 0,055$).

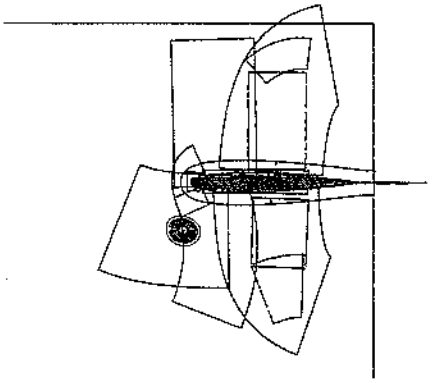

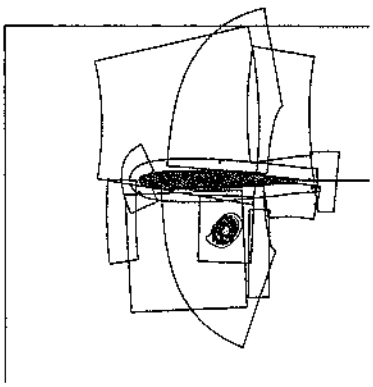

Figure 14: Vorticity contours at $t = 4,264\,\mathcal{T}$ et $t = 5,02\,\mathcal{T}$.

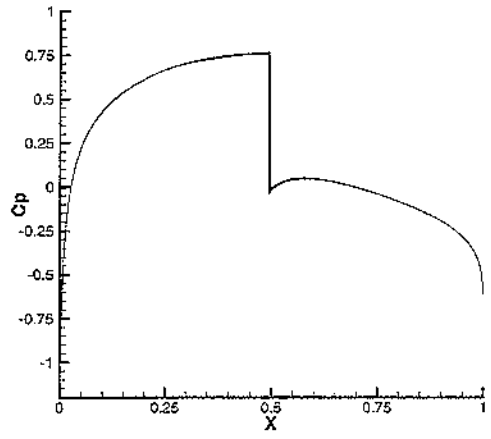

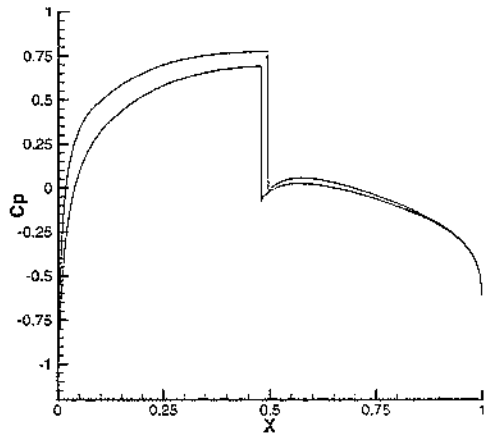

Figure 15: Pressure coefficient on the airfoil at $t = 0,18\,\mathcal{T}$, $t = 3,264\,\mathcal{T}$.

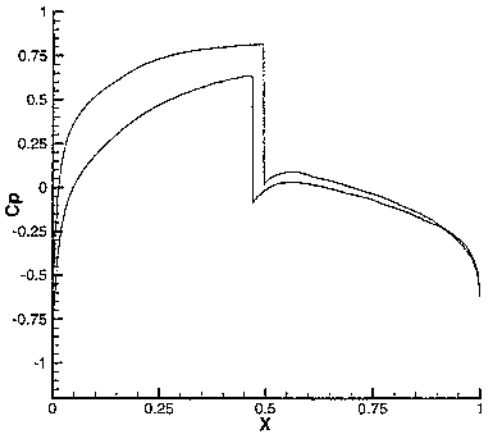

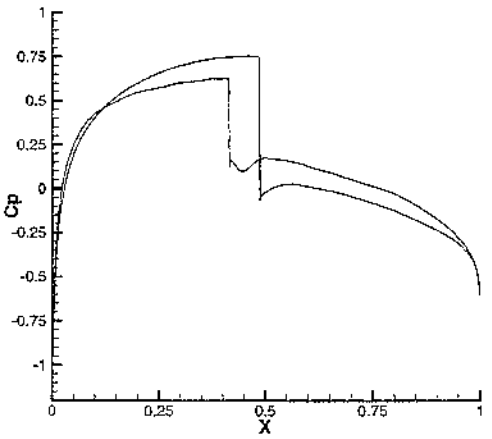

Figure 16: Pressure coefficient on the airfoil at $t = 4,264\,\mathcal{T}$ et $t = 5,02\,\mathcal{T}$.

However, additional effort should be devoted to improve efficiency of the method. They should concern particularily the optimization stage, where an important part of the CPU time is consumed.

Further work will be devoted to an extension of the method to 3D helicopter problems under the French-German CHANCE CFD project for the computation of a complete helicopter.

References

[1] J.A.BENEK, J.L.STEGER, F.C.DOUGHERTY, A Flexible Grid Embedding Technique with Application to the Euler Equations, 1983, AIAA Paper 83-1944.

[2] C.BENOIT, Méthode d'adaptation de maillages au moyen d'algorithmes génétiques pour le calcul d'écoulements compressibles, 1999, Thèse de doctorat ENSAM.

[3] M.BERGER, Adaptive Mesh Refinement for Partial Differential Equations, 1982, PhD Thesis, Stanford.

[4] J.H.HOLLAND, Adaption in Natural and Artificial Systems, 1975, Ann Arbor, University of Michigan Press.

[5] A.JAMESON, W.SCHMIDT, E.TURKEL, Numerical Solutions of the Euler Equations by Finite Volume Methods Using Runge-Kutta Time-Stepping Schemes, 1981, AIAA Paper 81-1259.

[6] A.LERAT, J.SIDÈS, V.DARU, An Implicit Finite-Volume Method for Solving the Euler Equations, 1982, Lecture Notes in Physics, vol. 170, pp. 343-349.

[7] N.LIAMIS, V.COUAILLIER, Unsteady Euler and Navier-Stokes Flow Simulations with an Implicit Runge-Kutta Method, 1994, 2^{nd} European CFD Conference ECCOMAS 94, Stuttgart.

[8] Z.MICHALEWICZ, Genetic Algorithms + Data Structures = Evolution Program, 1992, Springer Verlag.

[9] V.NASTASI, Etude numérique du tourbillon d'extrémité de pale du rotor d'hélicoptère en régime compressible, 1997, Thèse de doctorat ENSAM.

[10] N.L.NG, R.HILLIER, Numerical Simulation of the Transonic Blade-Vortex Interaction, 1996, 22^{nd} European Rotorcraft Forum, Brighton.

[11] A.OCHI, E.SHIMA, E.YAMAKAWA, T.AOYAMA, S.SAITO, Aerodynamic and Aeroacoustic Analysis of BVI by Moving Overlapped Grid Method, 1998, 24^{th} European Rotorcraft Forum, Marseilles, France.

[12] J.L.STEGER, D.S.CHAUSSEE, Generation of Body Fitted Coordinates Using Hyperbolic Partial Differential Equations, 1980, SIAM J. Sci. Stat. Comp., 1, pp. 431-437.

[13] G.R.SRINIVASAN, W.J. MCCROSKEY, J.D.BAEDER, Aerodynamics of the Two Dimensional Blade-vortex interaction, 1986, AIAA journal, 24, pp. 1569-1576.

[14] H.C.YEE, N.D.SANDHAM, M.J. DJOMEHRI, Low-Dissipative High-Order Shock-Capturing Methods Using Characteristic-Based Filters, 1999, Journal of Computational Physics 150, pp. 199-238.